



Published in final edited form as:

J Control Release. 2016 October 10; 239: 223–230. doi:10.1016/j.jconrel.2016.08.033.

Characterization of TCP-1 probes for molecular imaging of colon cancer

Zhonglin Liu^{a,*}, Brian D Gray^b, Christy Barber^a, Michael Bernas^c, Minying Cai^d, Lars R Furenlid^{a,h}, Andrew Rouse^a, Charmi Patel^e, Bhaskar Banerjee^{f,g,h}, Rongguang Liang^h, Arthur F Gmitro^{a,g,h}, Marlys H Witte^c, Koon Y Pak^b, and James M Woolfenden^a

^aDepartment of Medical Imaging, The University of Arizona, Tucson, AZ

^bMolecular Targeting Technologies, Inc., West Chester, PA

^cDepartment of Surgery, The University of Arizona, Tucson, AZ

^dDepartment of Chemistry & Biochemistry, The University of Arizona, Tucson, AZ

^eDepartment of Pathology, The University of Arizona, Tucson, AZ

^fDepartment of Medicine, The University of Arizona, Tucson, AZ

^gDepartment of Biomedical Engineering, The University of Arizona, Tucson, AZ

^hCollege of Optical Sciences, The University of Arizona, Tucson, AZ

Abstract

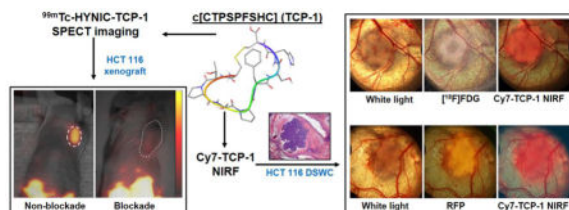
Molecular probes capable of detecting colorectal cancer (CRC) are needed for early CRC diagnosis. The objective of this study was to characterize c[CTPSPFSHC]OH (TCP-1), a small peptide derived from phage display selection, for targeting human CRC xenografts using technetium-99m (^{99m}Tc)-labeled TCP-1 and fluorescent cyanine-7 (Cy7)-labeled form of the peptide (Cy7-TCP-1). ^{99m}Tc-TCP-1 was generated by modifying TCP-1 with succinimidyl-6-hydrazino-nicotinamide (S-HYNIC) followed by radiolabeling. In vitro saturation binding experiments were performed for ^{99m}Tc-TCP-1 in human HCT116 colon cancer cells. SCID mice with human HCT116 cancer xenografts were imaged with ^{99m}Tc-TCP-1 or control peptide using a small-animal SPECT imager: Group I (n=5) received no blockade; Group II (n=5) received a blocking dose of non-radiolabeled TCP-1. Group III (n=5) were imaged with ^{99m}Tc-labeled control peptide (inactive peptide). SCID mice with human PC3 prostate cancer xenografts (Group IV, n=5) were also imaged with ^{99m}Tc-TCP-1. Eight additional SCID mice bearing HCT116 xenografts in dorsal skinfold window chambers (DSWC) were imaged by direct positron imaging of ¹⁸F-fluorodeoxyglucose (¹⁸F-FDG) and fluorescence microscopy of Cy7-TCP-1. *In vitro* ^{99m}Tc-HYNIC-TCP-1 binding assays on HCT 116 cells indicated a mean K_d of 3.04 ± 0.52 nM. In cancer xenografts, ^{99m}Tc-TCP-1 radioactivity (%ID/g) was 1.01±0.15 in the absence of

*For correspondence or reprints contact: P.O. Box 245067, Tucson, AZ 85724-5067, Phone: 520-626-4248; Fax: 520-626-2892, zliu@email.arizona.edu.

Publisher's Disclaimer: This is a PDF file of an unedited manuscript that has been accepted for publication. As a service to our customers we are providing this early version of the manuscript. The manuscript will undergo copyediting, typesetting, and review of the resulting proof before it is published in its final citable form. Please note that during the production process errors may be discovered which could affect the content, and all legal disclaimers that apply to the journal pertain.

blockade and was reduced to 0.26 ± 0.04 ($P < 0.01$) with blockade. No radioactive uptake was observed in the PC3 tumors with ^{99m}Tc -TCP-1 or HCT116 tumors with inactive peptide. Cy7-TCP-1 activity localized not only in metabolically active tumors, as defined by ^{18}F -FDG imaging, but also in peritumoral microvasculature. In conclusion, TCP-1 probes may have a distinct targeting mechanism with high selectivity for CRC and tumor-associated vasculature. Molecular imaging with TCP-1 probes appears promising to detect malignant colorectal lesions.

Graphical Abstract



Keywords

Colorectal cancer; molecular imaging; ^{99m}Tc ; SPECT; mouse xenograft models; peptide

1. Introduction

Colorectal cancer (CRC) is the third leading cause of cancer death in men and women in the United States [1]. Patients with inflammatory bowel disease (IBD), especially those with longstanding and extensive colitis such as ulcerative colitis or Crohn's disease, are at increased risk of developing invasive CRC compared to healthy individuals [2–4]. Periodic endoscopic surveillance with biopsy is commonly used in these populations to detect CRC and reduce CRC progression and mortality [5–7]. However, in approximately 5–10% of cases, complete visualization of the colonic mucosa is not achieved [8]. Visible findings at colonoscopy may lack morphologic detail and molecular specificity, and a dysplastic lesion may be difficult to distinguish from epithelial regeneration associated with inflammation. Dysplasia miss-rates with conventional colonoscopy have been reported as high as 22%. Thus, new imaging approaches with sensitive and specific molecular probes capable of differentiating colorectal CRC lesions from non-malignant lesions are clearly needed for early CRC detection [9–11].

The cyclic peptide c[Cys-Thr-Pro-Ser-Pro-Phe-Ser-His-Cys]OH (c[CTPSPFSHC]OH, TCP-1) was originally identified in orthotopic mouse CRC using phage display selection [12, 13]. It is bridged by a disulfide bond from the side chains of cysteine termini. A search for the lowest-energy conformation of the TCP-1 amino-acid sequence using MacroModel computational molecular modeling demonstrates that this cyclic peptide has a predominant β -sheet-like structure [14], as shown in Fig. 1, indicating that there is a relatively large binding region. *In vitro* and *in vivo* studies suggest that TCP-1 may have a unique ability to home to CRC neovasculature and deliver imaging agents and chemotherapeutic drugs to the tumor sites [12, 13, 15–17]. Cell imaging with TCP-1-conjugated quantum dots demonstrated that TCP-1 might localize in the nuclei [12, 13]. It is currently unclear if

TCP-1 is a nuclear localization signal (NLS) peptide, in which a protein is tagged for import into the cell nucleus by nuclear transport [12, 13], because the receptor for TCP-1 binding has not been identified. In preliminary studies using a mouse model with spontaneous CRC, we have found that a fluorescein isothiocyanate (FITC)-labeled TCP-1 probe was able to localize small cancer lesions by *ex vivo* microscopic imaging, but it did not localize in inflammatory tissues. To further evaluate whether TCP-1 peptide has high selectivity for CRC targeting, we labeled a TCP-1 peptide with radioisotope technetium-99m (^{99m}Tc) and also the near-infrared fluorophore cyanine-7 (Cy7) for molecular imaging. This study was designed to address the following three questions: First, were the TCP-1 probes able to specifically recognize human CRC? Second, did the TCP-1 probes selectively target to CRC only or did they also target other solid tumors, such as prostate cancer? Third, did the TCP-1 probes bind to both cancer cells and tumor vasculature? In order to answer these questions, we performed *in vitro* saturation-binding experiments of ^{99m}Tc -labeled TCP-1 peptide (^{99m}Tc -TCP-1) in human HCT116 colon cancer cells, collected *in vivo* imaging data of ^{99m}Tc -TCP-1 in xenografted HCT116 and PC3 prostate cancer model, and then used a dorsal skinfold window chamber (DSWC) to characterize the uptake profile of Cy7-TCP-1 in the HCT116 cancer and its neovasculature.

2. Materials and Methods

2.1. Probe preparation

The TCP-1 peptide was commercially synthesized at AnaSpec, Inc. (Fremont, CA) according to our specifications. CysValGlnThrAlaGlnLeuLeuCys (CVQTAQLLC) peptide was prepared to provide a negative control for characterizing the specificity of TCP-1 targeting. The TCP-1 and CVQTAQLLC peptides were prepared at purity > 95% at 254 nm by analytical high performance liquid chromatography (HPLC) and conjugated with succinimidyl 6-hydrazinopyridine-3-carboxylic acid (S-HYNIC) [18]. Low-resolution mass spectrometry (LRMS) was used to confirm the molecular weights of the HYNIC-labeled peptides. Observed mass for HYNIC-TCP-1 was 1151.1, with calculated mass of 1151.2; observed mass for HYNIC-CVQTAQLLC was 1152.2, with calculated mass of 1151.3. The resulting HYNIC-TCP-1 and HYNIC-CVQTAQLLC were formulated with N-(tri(hydroxymethyl)methyl)glycine (tricine) and ethylenediamine-N,N'-diacetic acid (EDDA) as co-ligands, and made into lyophilized kit forms for labeling with ^{99m}Tc .

2.2. Radiolabeling TCP-1 with ^{99m}Tc

Radiolabeling took place by adding pertechnetate ($^{99m}\text{TcO}_4^-$) in saline (55–740 MBq, 0.5 mL) to the vial containing 15 μg of HYNIC-TCP-1 or HYNIC-CVQTAQLLC, 30 mg of tricine, 10 mg of EDDA, and 15 μg of tin chloride dihydrate. The mixture was incubated for 30 minutes at 80°C. Radiolabeled products, ^{99m}Tc -TCP-1 and ^{99m}Tc -CVQTAQLLC, were purified by reverse-phase (RP) HPLC using a C18 column with a gradient elution of 0.1% trifluoroacetic acid (TFA) in water for the A-solvent and 0.1% TFA in acetonitrile (ACN) for the B-solvent at a flow rate of 1 mL/min. After HPLC purification, radiochemical purity (RCP) was greater than 99% for animal administration within 1 hour. *In vitro* stability of the radiolabeled peptides in mouse serum was tested by incubating 37 MBq of the radiolabeled product in 0.4 mL of mouse serum at 37°C for 1 and 6 hours, respectively. Subsequently, the

samples were centrifuged (4000 g, 4 °C) for 5 minutes, and 25 µL aliquots of the supernatant were analyzed by RP-HPLC [19].

2.3. Synthesis of Cy7 labeled TCP-1 (Cy7-TCP-1)

Cy7-TCP-1 was prepared by mixing a Cy7-carboxylic acid analog with TCP-1 at a molar ratio of 1:1 in anhydrous dimethyl sulfoxide (DMSO) in the presence of the O-(benzotriazol-1-yl)-N,N,N',N'-tetramethyluronium hexafluorophosphate (HBTU) and N,N-diisopropylethylamine. The reaction mixture was stirred for 2 hours and then purified by semi-preparative HPLC using a C18 column with water/acetonitrile/0.1% TFA gradient elution to provide pure Cy7-TCP-1 as a green solid after lyophilization. LRMS showed mass peak for Cy7-TCP-1 at 1847.0, with calculated mass of 1846.4 confirming the correct product was obtained.

2.4. In vitro saturation binding assay

The HCT116 human colon-cancer cell line was obtained from American Type Culture Collection (ATCC) (Rockville, MD). On the day prior to the experiment HCT116 cells (10^6 cells per well) were plated in 24-well plates and incubated at 37 °C and 5% CO₂ overnight. Cells were washed and media were replaced with binding media containing 1% BSA. ^{99m}Tc-TCP-1 with increasing concentrations (0.1–20 nM) was added to the wells and incubated with the cells at 37 °C for 2 hours. The total volume of each well was 0.8 ml. Nonspecific binding was determined by adding an excess of non-radiolabeled TCP-1 to each well 10 minutes prior to ^{99m}Tc-TCP-1. After incubation at 37 °C for 2 hours, the supernatant was removed and the cells were washed twice with 1 mL of ice-cold PBS (pH 7.4). The combined supernatants represent the free, unbound radiopeptide fraction. To determine cell-bound fraction, the cells were lysed with 1 M NaOH (1 mL) for 10 minutes at 37 °C and the wells were washed twice with 1 M NaOH (1 mL). The free and cell-bound fractions were measured in a gamma counter. Dissociation constants (K_d) were calculated from the data for specific binding with nonlinear regression using GraphPad Prism 6 (GraphPad Software, Inc., La Jolla, CA). Experimental conditions were performed in triplicate.

2.5. Xenografted tumor models and experimental groups

Severe combined immunodeficient (SCID) mice weighing 18–22 g were obtained from the mouse core facility at the University of Arizona Comprehensive Cancer Center to establish subcutaneous cancer xenografts. Mice were housed under pathogen-free conditions in microisolator cages with laboratory chow and water available. Human HCT116 colon cancer xenografts were established by subcutaneously injecting 9×10^6 HCT116 cancer cells into the mouse right shoulder. Similarly, PC3 human prostate-cancer cell xenografts were also established in SCID mice to serve as non-colon cancer controls. The PC3 cells were obtained from ATCC and cultured under standard conditions similar to HCT116 cells for subcutaneous implantation. The volumes of tumor were measured daily. After 7 to 10 days, tumors reached 5–15 mm in diameter and were studied in the following groups. **Group I:** Five mice carrying human HCT 116 colon cancer xenografts were imaged with ^{99m}Tc-HYNIC-TCP-1. **Group II:** Blocking tests were carried out in five mice with HCT116 xenografts by intravenous injection of 100-fold overdose of non-radiolabeled TCP-1 (100

μg , 0.2 mL) 5–10 minutes before $^{99\text{m}}\text{Tc}$ -TCP-1 administration. **Group III:** HCT116 xenografts in five mice were imaged with $^{99\text{m}}\text{Tc}$ -CVQTAQLLC inactive peptide. **Group IV:** Five mice bearing PC3 xenografts were imaged with $^{99\text{m}}\text{Tc}$ -TCP-1.

Dorsal skinfold window chambers (DSWC) were established in eight SCID mice [20, 21]. For implantation of the chamber into the dorsal skin, the entire back of the animal was shaved and depilated, and two symmetrical titanium frames were imbedded so as to sandwich the extended double layers of skin; one layer of skin was removed in a circular area approximately 15 mm in diameter, and the remaining layer was covered with a circular cover-glass incorporated into one of the frames. HCT116 and HCT116/RFP cells expressing red fluorescent protein (RFP) were implanted into the skinfold chamber to investigate the targeting selectivity of TCP-1 to the tumor lesion and tumor-associated vasculature by fluorescence imaging of Cy7-TCP-1. The cover-glass was carefully removed and cancer cells (2 μL , about 2×10^5 cells) were imbedded at the center of the chamber. A new cover-glass was then placed on the chamber. The tumors in the chamber model were grown for 5–7 days for imaging studies.

2.6. SPECT imaging of xenografted tumor models

Dynamic or static single-photon emission computed tomography (SPECT) images of all mice in Groups I-IV were acquired using a stationary SPECT imager, FastSPECT II [22]. FastSPECT II provides dynamic imaging capabilities without rotation of either animals or detectors. Each animal was anesthetized with 1.0–1.5% isoflurane, loaded into the FastSPECT II imager, and positioned so that the tumor on the right shoulder and the control left shoulder were in the field of view of the imager. $^{99\text{m}}\text{Tc}$ -TCP-1 or control peptide (55.5–92.5 MBq, 0.2 mL) was given by direct intravenous injection or administered using a pre-positioned catheter in the tail vein. Each mouse received approximately 1 μg HYNIC-conjugated peptide. In the Group I mice, dynamic SPECT list-mode projection data were collected every minute for 10 minutes immediately after tracer injection, followed by 5-minute projection data every 15 minutes up to 3 hours. All other mice in Groups II-IV were imaged once at 3 hours after tracer injection. Sixteen projections were obtained, one from each camera, to generate the data set for tomographic reconstruction. Reconstructions of FastSPECT II data were processed using 30 iterations of the maximum-likelihood estimation method (MLEM) algorithm. Tomographic transverse, coronal, and sagittal slices with one-voxel thickness (0.5 mm) were produced using AMIDE 1.0.4 software.

2.7. Imaging of DSWC models

Four mice with HCT116 xenografts in DSWC were imaged with ^{18}F -fluorodeoxyglucose (^{18}F -FDG) using a charged-particle imager. This imager was custom-built for imaging charged-particles emitted from tissues of a living organism [20, 21]. It consists of an ultra-thin phosphor capable of imaging radiolabeled tracers in superficial or exposed tissues, a high-numerical-aperture compound lens, and a cooled ultra-sensitive CCD camera. The mice were fasted for 6 hours before ^{18}F -FDG (37–74 MBq) was injected intravenously. A circular piece of phosphor was placed in direct contact with the xenografted tumor, vasculature, and skin within the chamber being imaged. Under anesthesia with 1.5% isoflurane, images of ^{18}F positron activity within the chamber were acquired for 5 minutes at 30–60 minutes

after ^{18}F -FDG injection. Cy7-TCP-1 (25 μg , 0.2 mL) was intravenously injected in the same mice approximately 24 hours after ^{18}F -FDG administration. White-light photographic and Cy7-TCP-1 fluorescent images of tissues within the chambers were acquired using a Nikon E600 microscope (Nikon Instruments Inc., Melville, NY) with an ICG filter (excitation 749 nm and emission 820 nm) for 5–8 seconds.

In order to further map the location of the tumor cells, tumor size, and vascular network related to TCP-1 uptake, Cy7-TCP-1 was injected and imaged using the ICG filter as described above in four anesthetized mice bearing HCT116/RFP xenografts, and then fluorescence of RFP-expressing tumor cells within the chamber was imaged using the same microscope with a DSRed2 filter set (excitation 558 nm and emission 583 nm) for 1–5 seconds.

2.8. Postmortem assays

All mice in Groups I-IV were sacrificed by barbiturate overdose at the end of the imaging session, and samples of tumor, blood, kidney, liver, heart, lung and skeletal muscle were harvested. The tissue samples were weighed and the radioactivity was measured by the CRC-15W Dose Calibrator/Well Counter (Capintec, Inc., Ramsey, NJ) to calculate the percentage of injected dose per gram of tissue (%ID/g). In the mice with DSWC, the titanium frames were removed and the skin with tumors inside the chambers was harvested. The tumors were excised and fixed in formalin-saline for 24 hours. After paraffin mounting, sections (5 μm) were cut, stained with hematoxylin and eosin (H&E), and examined microscopically.

2.9. Statistical analysis

All quantitative results were expressed as mean \pm S.E.M. Comparisons between two variables were performed with one-way analysis of variance. Probability values less than 0.05 were considered significant.

2.10. Ethics

The animal experiments were performed in accordance with Principles of Laboratory Animal Care from the National Institutes of Health (NIH Publication 85-23, revised 1985) and were approved by the Institutional Animal Care and Use Committee (IACUC) at the University of Arizona.

3. Results

3.1. Radiolabeling, in vitro stability, and cell binding

The labeling yield of the product was 92–95% and the radiochemical purity was greater than 99% after HPLC purification. A representative HPLC radiochromatogram of $^{99\text{m}}\text{Tc}$ -TCP-1 is shown in Fig. 2a. The retention times were 5.12 minutes for $^{99\text{m}}\text{TcO}_4^-$ and 16.64 minutes for $^{99\text{m}}\text{Tc}$ -TCP-1. After 1 hour and 6 hours of incubation at 37°C, more than 98% and 95% of $^{99\text{m}}\text{Tc}$ -HYNIC-TCP-1, respectively, remained intact in saline or mouse serum, as shown in Fig. 2b and Fig. 2c. The major species produced in plasma was $^{99\text{m}}\text{TcO}_4^-$, with a retention time of approximately 5.12 minutes. Its identity was confirmed by a retention time identical

to that of authentic sodium ^{99m}Tc -pertechnetate. There was no evidence of any metabolism occurring in serum. The radiolabeling of HYNIC-CVQTAQLLC with ^{99m}Tc yielded similar result and stability.

In vitro saturation binding of ^{99m}Tc -TCP-1 on HCT-116 cells demonstrated a mean K_d of 3.04 ± 0.52 nM. A related saturation curve is shown in Fig. 3.

3.2. SPECT images of HCT116 and PC3 cancer xenografts

As shown in Fig. 4, dynamic images of ^{99m}Tc -TCP-1 in the mice of Group I with HCT116 colon cancer xenografts demonstrated that the tumor could be initially localized by 15–30 minutes after injection and remained readily detectable at the end of the imaging session at 180 minutes. Relative to the animals with non-blockade (Fig. 5a), *in vivo* blockade by unlabeled TCP-1 induced a significant decrease in HCT116 tumor uptake of ^{99m}Tc -TCP-1, as shown in Fig. 5b. The ^{99m}Tc -CVQTAQLLC control peptide exhibited no activity above background, as shown in Fig. 5c. When ^{99m}Tc -TCP-1 was administered in mice bearing human prostate cancer, images showed that the radioactivity of the PC3 prostate cancer xenografts in Group IV animals was at the level of soft tissue background activity (Fig. 5d).

3.3. Results of biodistribution measurements

Postmortem biodistribution measurements (%ID/g) are summarized in Table 1. ^{99m}Tc -TCP-1 showed prominent renal excretion and low uptake in the liver and gut in the mice of Groups I-IV. The HCT116 tumors in Group I accumulated significantly higher radioactivity of ^{99m}Tc -TCP-1 than blood, muscle, and skin ($P < 0.01$). Cold ligand blockade in Group II reduced ^{99m}Tc -TCP-1 tumor uptake significantly ($P = 0.001$). Similarly, mice in Group III receiving ^{99m}Tc -CVQTAQLLC inactive peptide showed significantly less radioactivity in the HCT116 tumors ($P = 0.002$), but higher blood activity ($P < 0.001$) and kidney uptake ($P < 0.05$) compared to animals in Group I that received ^{99m}Tc -TCP-1. Uptake of ^{99m}Tc -TCP-1 in the xenografted PC3 prostate cancer was significantly lower than that in the HCT116 cancer ($P < 0.001$). The radioactive ratios of tumor to blood and muscle were statistically higher in the HCT116 tumors without blockade than that in the tumors of other three groups ($P < 0.01$, respectively).

3.4. TCP tumor uptake in the DSWC model

White-light imaging of the DSWC showed the areas of implanted tumor cells and associated blood vessels (Fig. 6a and d). Capillaries near the boundary zone of the HCT116 tumor lesion were also visible. The area of active tumor metabolic activity, indicated by ^{18}F -FDG uptake (Fig. 6b), was smaller than the anatomical lesion size delineated on the microscopic white-light image in Fig. 6a. In two of the four mice with HCT116 DSWC, the ^{18}F -FDG image taken by the direct positron imager revealed an annular shape of the radioactive accumulation, as in Fig. 6b. Subsequent pathological analysis indicated that the high ^{18}F -FDG uptake was associated with areas of dense and rapidly growing tumor cells. There were mismatches in Cy7-TCP-1 distribution on the fluorescence image (Fig. 6c) and ^{18}F -FDG uptake on direct positron image taken one day earlier (Fig. 6b). Fluorescence microscopy demonstrated that the area of Cy7-TCP-1 uptake was larger than ^{18}F -FDG tumor uptake and covered both the tumor mass and a peripheral rim consisting of blood vessels, capillaries,

and connective tissue. In the DWSC with implanted HCT116 cells expressing red fluorescent protein, the location and extent of Cy7-TCP-1 uptake (Fig. 6f) extended beyond the RFP-positive tumoral lesion (Fig. 6e) and corresponded to the extent of the anatomical lesion seen on white-light examination (Fig. 6d). Overall, the Cy7-TCP-1 activity was found to localize within the tumor lesion, peritumoral microvasculature, and some tumor-associated vessels, as illustrated on co-registered fluorescence and white light microscopic images in Fig. 6 a&c and d&f.

3.5. Histologic findings

H & E staining of the skin and tumor from the DWSC showed that the tumor was composed of hyperchromatic polyhedral, ovoid and spheroidal cells arranged in sheets. The tumor cells displayed fairly prominent nucleoli, high nuclear to cytoplasmic ratios and many mitotic figures. The tumor boundary zone was composed of a mixture of newly formed blood vessels, collagen, and various stromal cells including adipocytes, fibroblasts, lymphocytes, mast cells, and macrophages. The underlying blood vessels on the tumor edge exhibited proliferation with irregular chaotic, looped and blunt ends. Representative photomicrographs of HCT116 and HCT116/RFP tumors in DSWCs are shown in Fig. 7.

4. Discussion

When TCP-1 was originally identified from mouse CRC, initial studies focused on evidence of TCP-1 targeting CRC vasculature [12, 13]. It was also found that TCP-1 was able to react with human CRC and target the blood vessels of human CRC samples. Although the specific target for TCP-1 has not been elucidated, it is possible that TCP-1 receptors are expressed on both CRC cells and stromal endothelial cells, since tumor cells, tumor-associated and tumor-derived endothelial cells share biomarkers [23, 24]. The TCP-1 receptors may be unique to these neoplastic cells [13, 25, 26], or they may be expressed at low levels in healthy tissues but elevated in malignant tissues. Based on our results, it can be reasonably expected that ^{99m}Tc -TCP-1 molecular imaging should be able to localize human CRC by targeting both tumor cells and tumor-associated vasculature. Radiolabeled or fluorescent-labeled TCP-1 probes that simultaneously recognize both cancer cells and tumor vasculature might offer an advantage over probes that target only cancer cells or blood vessels by exploiting an increased number of targets.

Our studies of ^{99m}Tc -TCP-1 *in vitro* cell binding showed selectivity for CRC, consistent with results in a previous report [12]. The reduced ^{99m}Tc -TCP-1 tumor uptake in animals receiving TCP-1 blockade under the same experimental conditions is also consistent with specific targeting. The lack of ^{99m}Tc -TCP-1 uptake in human PC3 prostate cancer xenografts suggests that TCP-1 is likely a specific biomarker for CRC or gastrointestinal cancers but not for other solid tumors. However, further studies with additional human cancer cell lines are also warranted.

Results with the inactive peptide, ^{99m}Tc -CVQTAQLLC, also support specificity of ^{99m}Tc -TCP-1 in the HCT116 xenografts. The tumor xenografts showed only slightly increased uptake of inactive peptide relative to muscle, probably caused by increased tumor vascular permeability. The radiopharmaceutical profile of ^{99m}Tc -CVQTAQLLC is not identical

to ^{99m}Tc -TCP-1, as shown by its higher blood retention and kidney uptake. This biodistribution difference might be due to different hydrophilic properties of these two peptides. It is also possible that the higher kidney accumulation resulted from absence of uptake of the inactive control peptide in the tumor, with increased peptide available for renal excretion.

Uptake of ^{99m}Tc -TCP-1 was prominently associated with areas of rapidly growing tumor cells, and there was lack of uptake in slowly growing and necrotic tumor areas. It is possible that TCP-1 uptake is associated with angiogenesis in the metabolically active tumor sites, but it appears to be different from Arg-Gly-Asp (RGD) targeting of integrin $\alpha_v\beta_3$ [27, 28]. Targeting of RGD peptide is independent of tumor type because integrin $\alpha_v\beta_3$ receptors are present at low levels in normal vasculature and upregulated during angiogenesis on all types of blood vessels [29, 30]. Increased permeability of tumor vasculature is not a major cause of increased ^{99m}Tc -TCP-1 uptake in the HCT116 colon tumors, based on the specific binding results described above and the absence of uptake of the radiolabeled control peptide. Unfortunately, because the TCP-1 receptor is still unidentified, we have not been able to quantify receptor expression for characterization of TCP-1 targeting.

In SPECT or PET imaging, the route of excretion of the radioligand may potentially interfere with observation of abdominal and pelvic tumors. Like other hydrophilic radiolabeled peptides, ^{99m}Tc -TCP-1 is excreted mainly via the kidneys and results in high renal retention, with less uptake in liver and intestines. Renal retention might also be caused in part by reabsorption in proximal tubular cells. Molecular modification of the TCP-1 peptide and competitive inhibition of its renal reabsorption may be exploited to reduce the radioactivity in the kidneys [31, 32]. Different ^{99m}Tc chelators as well as linking groups that affect the overall hydrophilicity and charge of the tracer may improve biodistribution. In future studies we will investigate whether the kidney uptake of ^{99m}Tc -TCP-1 can be overcome by co-administration of cationic amino acids such as lysine or arginine [32].

Current CRC diagnostic methods have lacked practical molecular imaging probes [7, 33, 34]. SPECT imaging with ^{99m}Tc -TCP-1 may offer unique features relative to other CRC imaging methods such as immunoscintigraphy and ^{18}F -FDG PET imaging in discriminating early CRC lesions from inflammatory tissues [9]. Although radiolabeled antibodies or antibody fragments can target CRC primary tumor sites and metastases with high specificity and good predictive value [35–37], there are drawbacks to the use of antibodies, including cost, immune response on repeat administration, suboptimal pharmacokinetics, and hepatobiliary excretion that results in high radioactive background in the intestine [35]. Some of these disadvantages can be overcome by using engineered or humanized antibody fragments. However, the utility of radiolabeled engineered antibody fragments for CRC diagnosis has not yet been clarified. PET imaging with ^{18}F -FDG is widely used for staging CRC and detecting recurrent or metastatic CRC sites [38, 39]. However, ^{18}F -FDG is taken up by all metabolically active cells and inflammatory tissues [9, 40], making distinction difficult between inflammatory sites and tumors in the setting of bowel inflammation. Because of its small size and stable binding affinity, TCP-1 is expected to be able to penetrate tumor tissues and recognize targets more efficiently than antibodies. ^{99m}Tc -TCP-1 may reach clinically acceptable target-to-nontarget ratios quickly because of its rapid blood

clearance and low uptake in liver and normal gastrointestinal tract, as shown by our data in this study. Moreover, unlike most molecular imaging probes that bind to receptors on the tumor cell surface, it is believed that the TCP-1-based probes may undergo endocytosis and distribute mainly in the nucleus [12, 13], with the result that the probes may be retained longer than cell-surface ligands.

Our studies exploited the capability of DSWC to spatially co-register multiple parameters including tumor cell location, metabolism, and the microvasculature. The direct comparison of spatially-co-registered fluorescence and ^{18}F -FDG images in the DSWC allowed us to identify both tumoral and vascular Cy7-TCP-1 uptake. The Cy7-TCP-1 uptake in the tumor-associated vasculature, particularly on the tumor margin with high microvessel density, suggests that TCP-1 receptors may be expressed on both cancer cells and endothelial cells. The tumor vascular uptake of Cy7-TCP-1 might represent a specific biomarker expressed on endothelial cell phenotypes promoted by or derived from the colon cancer cells. Tumor cells can release angiogenic factors into their surrounding environment to promote new vessel growth [41]. Stem-like tumor cells can directly transdifferentiate into endothelial cells *in vivo* [23]. The tumor cells can also secrete exosomes that carry genetic information including mRNA, miRNA, and proteins capable of activating endothelial cells within their microenvironment [41–43]. Thus, the implanted HCT116 cells and tumor endothelial cells might share the molecular targets of TCP-1.

TCP-1 imaging methods have potentially high significance for clinical translation, particularly in the setting of inflammatory bowel disease. TCP-1 SPECT imaging that suggests the presence of CRC could be followed by endoscopic methods such as fluorescence-guided or confocal endoscopy for precise localization for biopsy. Further characterization and optimization of the TCP-1 molecular imaging probes may result in diagnostic agents that improve the specific detection of early-stage tumors and thereby lead to decreased CRC mortality.

5. Conclusion

TCP-1 represents an innovative targeting molecule for detecting CRC and its vasculature. We have collected *in vivo* data of the first $^{99\text{m}}\text{Tc}$ -labeled TCP-1 probe and its near-infrared fluorescent analog, Cy7-TCP-1, which demonstrate the feasibility of TCP-1-targeted detection of colorectal tumor xenografts. The TCP-1 probes localized in the metabolically active portion of the tumor and also in the tumor-associated vasculature. Further studies of the mechanism of TCP-1 binding are warranted, as are studies to verify detection of orthotopic and spontaneous CRC in animal models.

Acknowledgments

The authors are grateful to Dr. Harrison Barrett, Director of the Center for Gamma-Ray Imaging, for making the facilities of the Center available for animal imaging studies. We wish to thank Dr. Gail Stevenson for support in animal care and Dr. Luca Caucci for expertise in SPECT data reconstruction.

This work was supported by the National Institutes of Health [NIBIB P41-EB002035] and a grant from the Arizona Area Health Education Centers (AHEC) Program. It is noted that the content is solely the responsibility of the authors and does not necessarily represent the official views of Arizona AHEC.

References

1. Siegel R, Desantis C, Jemal A. Colorectal cancer statistics, 2014. *CA Cancer J Clin.* 2014; 64:104–117. [PubMed: 24639052]
2. Hsiung PL, Hardy J, Friedland S, Soetikno R, Du CB, Wu AP, Sahbaie P, Crawford JM, Lowe AW, Contag CH, Wang TD. Detection of colonic dysplasia in vivo using a targeted heptapeptide and confocal microendoscopy. *Nature medicine.* 2008; 14:454–458.
3. Carns J, Keahey P, Quang T, Anandasabapathy S, Richards-Kortum R. Optical molecular imaging in the gastrointestinal tract. *Gastrointestinal endoscopy clinics of North America.* 2013; 23:707–723. [PubMed: 23735112]
4. Triantafillidis JK, Nasioulas G, Kosmidis PA. Colorectal cancer and inflammatory bowel disease: epidemiology, risk factors, mechanisms of carcinogenesis and prevention strategies. *Anticancer research.* 2009; 29:2727–2737. [PubMed: 19596953]
5. Farraye FA, Odze RD, Eaden J, Itzkowitz SH, McCabe RP, Dassopoulos T, Lewis JD, Ullman TA, James T 3rd, McLeod R, Burgart LJ, Allen J, Brill JV. A.G.A.I.M.P.P.o. Diagnosis, D. Management of Colorectal Neoplasia in Inflammatory Bowel, AGA medical position statement on the diagnosis and management of colorectal neoplasia in inflammatory bowel disease. *Gastroenterology.* 2010; 138:738–745. [PubMed: 20141808]
6. Awais D, Siegel CA, Higgins PD. Modelling dysplasia detection in ulcerative colitis: clinical implications of surveillance intensity. *Gut.* 2009; 58:1498–1503. [PubMed: 19651634]
7. Kim ER, Chang DK. Colorectal cancer in inflammatory bowel disease: the risk, pathogenesis, prevention and diagnosis. *World journal of gastroenterology : WJG.* 2014; 20:9872–9881. [PubMed: 25110418]
8. Aslinia F, Uradomo L, Steele A, Greenwald BD, Raufman JP. Quality assessment of colonoscopic cecal intubation: an analysis of 6 years of continuous practice at a university hospital. *The American journal of gastroenterology.* 2006; 101:721–731. [PubMed: 16494586]
9. Turker NS, Heidari P, Kucherlapati R, Kucherlapati M, Mahmood U. An EGFR targeted PET imaging probe for the detection of colonic adenocarcinomas in the setting of colitis. *Theranostics.* 2014; 4:893–903. [PubMed: 25057314]
10. Miller SJ, Joshi BP, Feng Y, Gaustad A, Fearon ER, Wang TD. In vivo fluorescence-based endoscopic detection of colon dysplasia in the mouse using a novel peptide probe. *PLoS one.* 2011; 6:e17384. [PubMed: 21408169]
11. Liu Z, Miller SJ, Joshi BP, Wang TD. In vivo targeting of colonic dysplasia on fluorescence endoscopy with near-infrared octapeptide. *Gut.* 2013; 62:395–403. [PubMed: 22427239]
12. Li ZJ, Cho CH. Peptides as targeting probes against tumor vasculature for diagnosis and drug delivery. *Journal of translational medicine.* 2012; 10(Suppl 1):S1. [PubMed: 23046982]
13. Li ZJ, Wu WK, Ng SS, Yu L, Li HT, Wong CC, Wu YC, Zhang L, Ren SX, Sun XG, Chan KM, Cho CH. A novel peptide specifically targeting the vasculature of orthotopic colorectal cancer for imaging detection and drug delivery. *Journal of controlled release : official journal of the Controlled Release Society.* 2010; 148:292–302. [PubMed: 20854857]
14. Kolossvary I, Guida WC. Low-mode conformational search elucidated: Application to C39H80 and flexible docking of 9-deazaguanine inhibitors into PNP. *J Comput Chem.* 1999; 20:1671–1684.
15. Lu L, Li ZJ, Li LF, Wu WK, Shen J, Zhang L, Chan RL, Yu L, Liu YW, Ren SX, Chan KM, Cho CH. Vascular-targeted TNFalpha improves tumor blood vessel function and enhances antitumor immunity and chemotherapy in colorectal cancer. *Journal of controlled release : official journal of the Controlled Release Society.* 2015; 210:134–146. [PubMed: 26003042]
16. Shen J, Li ZJ, Li LF, Lu L, Xiao ZG, Wu WK, Zhang L, Li MX, Hu W, Chan KM, Cho CH. Vascular-targeted TNFalpha and IFNgamma inhibits orthotopic colorectal tumor growth. *Journal of translational medicine.* 2016; 14:187. [PubMed: 27342639]
17. Conde J, Oliva N, Zhang Y, Artzi N. Local triple-combination therapy results in tumour regression and prevents recurrence in a colon cancer model. *Nat Mater.* 2016
18. Meszaros LK, Dose A, Biagini SC, Blower PJ. Synthesis and evaluation of analogues of HYNIC as bifunctional chelators for technetium. *Dalton Trans.* 2011; 40:6260–6267. [PubMed: 21350776]

19. Erfani M, Zarrabi Ahrabi N, Shafiei M, Shirmardi SP. A (99m) Tc-tricine-HYNIC-labeled peptide targeting the neurotensin receptor for single-photon imaging in malignant tumors. *J Labelled Comp Radiopharm*. 2014; 57:125–131. [PubMed: 24395489]
20. Chen L, Gobar LS, Knowles NG, Liu Z, Gmitro AF, Barrett HH. Direct imaging of radionuclide-produced electrons and positrons with an ultrathin phosphor, *Journal of nuclear medicine : official publication. Society of Nuclear Medicine*. 2008; 49:1141–1145.
21. Chen L, Gobar LS, Knowles NG, Wilson DW, Barrett HH. Direct Charged-Particle Imaging System Using an Ultra-Thin Phosphor: Physical Characterization and Dynamic Applications. *IEEE transactions on nuclear science*. 2009; 56:2628–2635. [PubMed: 20191098]
22. Furenlid LR, Wilson DW, Chen YC, Kim H, Pietraski PJ, Crawford MJ, Barrett HH. FastSPECT II: A Second-Generation High-Resolution Dynamic SPECT Imager. *IEEE Trans Nucl Sci*. 2004; 51:631–635. [PubMed: 20877439]
23. McGuire TF, Sajithlal GB, Lu J, Nicholls RD, Prochowik EV. In vivo evolution of tumor-derived endothelial cells. *PLoS One*. 2012; 7:e37138. [PubMed: 22623986]
24. Meseure D, Drak Alsibai K, Nicolas A. Pivotal role of pervasive neoplastic and stromal cells reprogramming in circulating tumor cells dissemination and metastatic colonization. *Cancer Microenviron*. 2014; 7:95–115. [PubMed: 25523234]
25. Laakkonen P, Zhang L, Ruoslahti E. Peptide targeting of tumor lymph vessels. *Ann N Y Acad Sci*. 2008; 1131:37–43. [PubMed: 18519957]
26. Oh P, Li Y, Yu J, Durr E, Krasinska KM, Carver LA, Testa JE, Schnitzer JE. Subtractive proteomic mapping of the endothelial surface in lung and solid tumours for tissue-specific therapy. *Nature*. 2004; 429:629–635. [PubMed: 15190345]
27. Sezeur A, Chatelet FP, Cywiner C, de Labriolle-Vaylet C, Chastang C, Billotey C, Malafosse M, Gallot D, Betton P, Montravers F, Carvajal-Gonzalez S, Askienazy S, Talbot JN, Rain JD, Milhaud G, Saumon G, Barbet J, Gruaz-Guyon A. Pathology underrates colon cancer extranodal and nodal metastases; ex vivo radioimmunodetection helps staging. *Clinical cancer research : an official journal of the American Association for Cancer Research*. 2007; 13:5592s–5597s. [PubMed: 17875794]
28. Maruta F, Akita N, Nakayama J, Miyagawa S, Ismail T, Rowlands DC, Kerr DJ, Fisher KD, Seymour LW, Parker AL. Bacteriophage biopanning in human tumour biopsies to identify cancer-specific targeting ligands. *Journal of drug targeting*. 2007; 15:311–319. [PubMed: 17487700]
29. Laakkonen P, Vuorinen K. Homing peptides as targeted delivery vehicles. *Integrative biology : quantitative biosciences from nano to macro*. 2010; 2:326–337. [PubMed: 20657951]
30. Niu G, Chen X. Why integrin as a primary target for imaging and therapy. *Theranostics*. 2011; 1:30–47. [PubMed: 21544229]
31. Vegt E, de Jong M, Wetzels JF, Masereeuw R, Melis M, Oyen WJ, Gotthardt M, Boerman OC. Renal toxicity of radiolabeled peptides and antibody fragments: mechanisms, impact on radionuclide therapy, and strategies for prevention. *J Nucl Med*. 2010; 51:1049–1058. [PubMed: 20554737]
32. Gotthardt M, van Eerd-Vismale J, Oyen WJ, de Jong M, Zhang H, Rolleman E, Maecke HR, Behe M, Boerman O. Indication for different mechanisms of kidney uptake of radiolabeled peptides. *J Nucl Med*. 2007; 48:596–601. [PubMed: 17401097]
33. Schottelius M, Wester HJ. Molecular imaging targeting peptide receptors. *Methods*. 2009; 48:161–177. [PubMed: 19324088]
34. Kiesslich R, Hoffman A, Neurath MF. Colonoscopy, tumors, and inflammatory bowel disease - new diagnostic methods. *Endoscopy*. 2006; 38:5–10. [PubMed: 16429347]
35. Ramos-Suzarte M, Pintado AP, Mesa NR, Oliva JP, Iznaga-Escobar N, Aroche LT, Pimentel G, Gonzalez J, Cordero M, Rodriguez OT, Crombet RT, Perez RR. Diagnostic efficacy and safety of 99mTc-labeled monoclonal antibody ior c5 in patients with colorectal and anal carcinomas: final report clinical trial phase I/II. *Cancer biology & therapy*. 2007; 6:22–29. [PubMed: 17224642]
36. Erb DA, Nabi HA. Clinical and technical considerations for imaging colorectal cancers with technetium-99m-labeled antiCEA Fab' fragment. *Journal of nuclear medicine technology*. 2000; 28:12–18. quiz 21. [PubMed: 10763776]

37. Artiko VM, Sobic-Saranovic DP, Krivokapic ZV, Petrovic MN, Obradovic VB. Is there a future role for immunoscintigraphy in the diagnosis of colorectal carcinoma? *Neoplasma*. 2009; 56:1–8. [PubMed: 19152238]
38. Chowdhury FU, Shah N, Scarsbrook AF, Bradley KM. [18F]FDG PET/CT imaging of colorectal cancer: a pictorial review. *Postgrad Med J*. 2010; 86:174–182. [PubMed: 20237012]
39. Liong SY, Kochhar R, Renehan AG, Manoharan P. Utility of 18-fluorodeoxyglucose positron emission/computed tomography in the management of recurrent colorectal cancer. *ANZ J Surg*. 2012; 82:729–736. [PubMed: 22989147]
40. Liu D, Overbey D, Watkinson LD, Smith CJ, Daibes-Figueroa S, Hoffman TJ, Forte LR, Volkert WA, Giblin MF. Comparative evaluation of three ⁶⁴Cu-labeled *E. coli* heat-stable enterotoxin analogues for PET imaging of colorectal cancer. *Bioconjugate chemistry*. 2010; 21:1171–1176. [PubMed: 20536242]
41. Yamada N, Tsujimura N, Kumazaki M, Shinohara H, Taniguchi K, Nakagawa Y, Naoe T, Akao Y. Colorectal cancer cell-derived microvesicles containing microRNA-1246 promote angiogenesis by activating Smad 1/5/8 signaling elicited by PML down-regulation in endothelial cells. *Biochimica et biophysica acta*. 2014; 1839:1256–1272. [PubMed: 25218966]
42. D'Souza-Schorey C, Clancy JW. Tumor-derived microvesicles: shedding light on novel microenvironment modulators and prospective cancer biomarkers. *Genes Dev*. 2012; 26:1287–1299. [PubMed: 22713869]
43. Valadi H, Ekstrom K, Bossios A, Sjostrand M, Lee JJ, Lotvall JO. Exosome-mediated transfer of mRNAs and microRNAs is a novel mechanism of genetic exchange between cells. *Nat Cell Biol*. 2007; 9:654–659. [PubMed: 17486113]

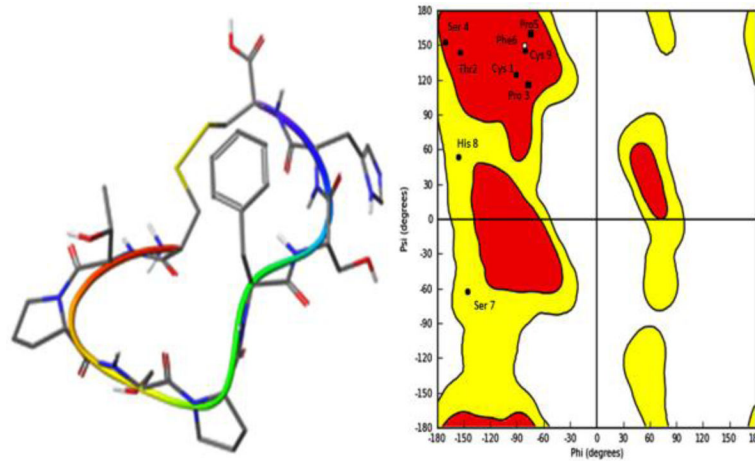


Fig. 1. *Left panel:* The lowest-energy conformation of c[CTPSPFSHC] (TCP-1). It shows a β -sheet-like structure. *Right panel:* Ramachandran plot of TCP-1 demonstrates that the majority of amino acids sit in the red region corresponding to the β -sheet region. His⁸ and Ser⁷ are in the yellow region corresponding to the random coil region, but close to the right handed α -helix. The plot calculation was done with Macro Model program.

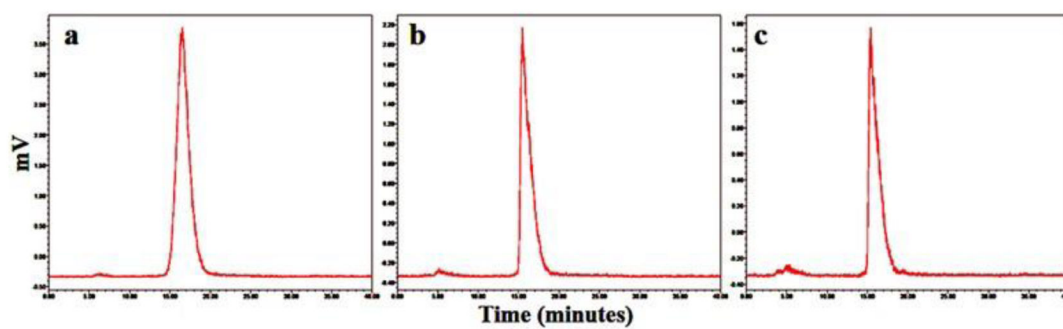


Fig. 2. Representative HPLC radiochromatograms of $^{99\text{m}}\text{Tc}$ -TCP-1 immediately after purification in saline (*a*) and after incubation at 37°C in mouse serum for 1 hour (*b*) and 6 hours (*c*).

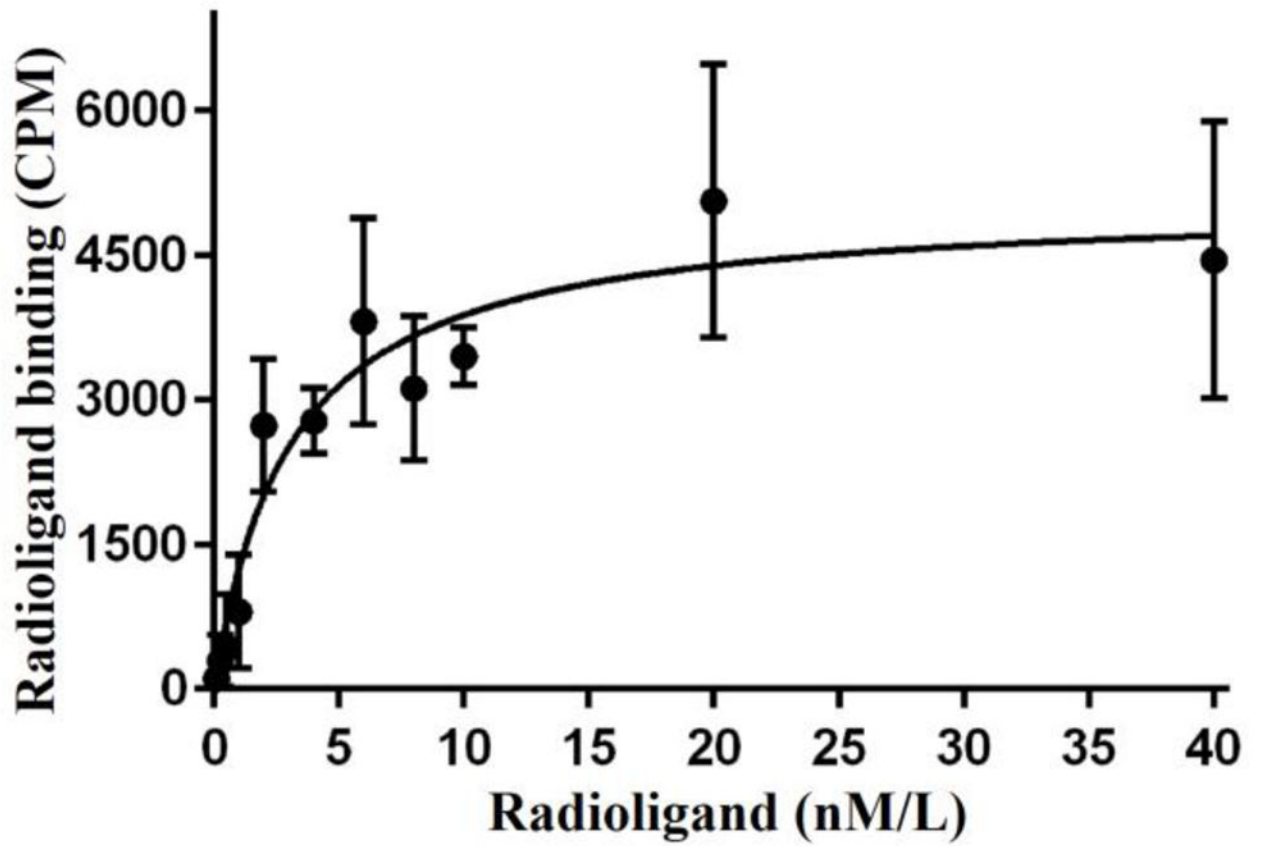


Fig. 3. Saturation curve for binding of ^{99m}Tc -TCP-1 to HCT116 colon cancer cells. The mean K_d was 3.04 ± 0.52 nM.

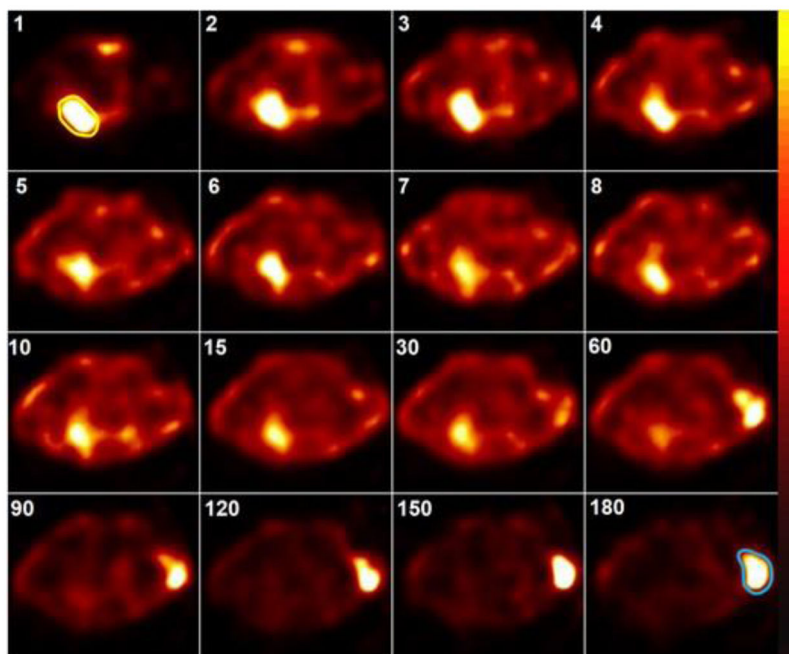


Fig. 4. Dynamic images (serial transversal slices) of ^{99m}Tc -TCP-1 in a SCID mouse bearing HCT116 colon cancer xenograft. The numbers in the upper left corners represent the minutes after injection. Immediately after radiotracer injection, cardiac blood pool was evident, as outlined in yellow on the 1-minute image, and remained visible up to at least 30 minutes. Tumor implanted on the right shoulder became visible about 10–15 minutes after injection, with increasing ratio of tumor to background activity from 60 to 180 minutes. The tumor is outlined in blue on the 180-minute image.

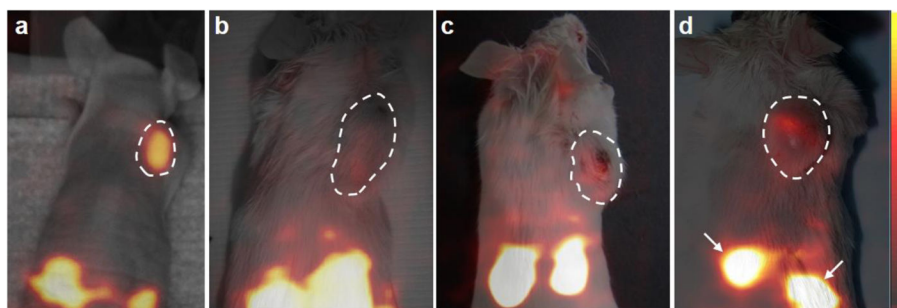


Fig. 5. Representative volume-rendered data sets in three-dimensional display of SPECT images co-registered with photographs of four mice with cancer xenografts, with each tumor outlined in white. The mouse with HCT116 xenograft (*a*), which received no blockade, demonstrated higher uptake of ^{99m}Tc -TCP-1 in the tumor compared to the mouse with HCT116 tumor receiving unlabeled TCP-1 blockade (*b*), xenografted HCT116 tumor imaged by inactive ^{99m}Tc -CVQTAQLLC (*c*), and the PC3 prostate cancer imaged by ^{99m}Tc -TCP-1 (*d*). High uptake of radioactivity is also seen in the kidneys as marked by arrows.

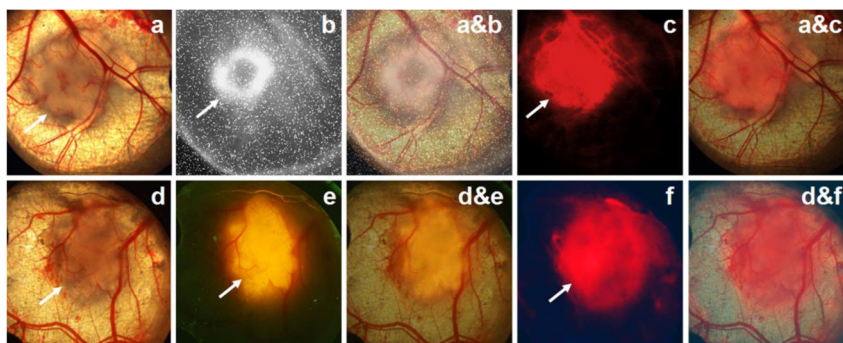


Fig. 6. Images of the DSWC model. **Top row:** (a) White-light photomicrograph of HCT116 cells growing in the window chamber. Underlying blood vessels are clearly visible. The site of implanted tumor cells along with peritumoral microvasculature is defined as the tumor anatomical lesion. (b) ^{18}F -FDG direct positron image of the window chamber in a showing the area of tumor metabolic activity. ^{18}F -FDG uptake exhibits annular distribution with smaller size relative to the anatomical lesion observed by microscopy. (a&b) Co-registered image of a and b. (c) Cy7-TCP-1 fluorescence microscopic image corresponding to the window-chamber image in a. (a&c) Co-registered image of a and c. The Cy7 fluorescence signal co-localizes with the anatomical lesion. Cy7-TCP-1 uptake also corresponds to some blood vessels associated with the tumor. **Bottom row:** (d) White-light photomicrograph of window chamber with implanted HCT116/RFP cells with red fluorescent protein expression. (e) Corresponding red fluorescence image of window chamber in d. (d&e) Co-registered image of d and e. The area of RFP-expressing cells is smaller than the anatomical lesion under white-light illumination. (f) Cy7-TCP-1 fluorescence image in the same window chamber as d. (d&f) Co-registered image of d and f. The area of Cy7 fluorescence corresponds to the anatomical lesion but is larger than the area of RFP expression.

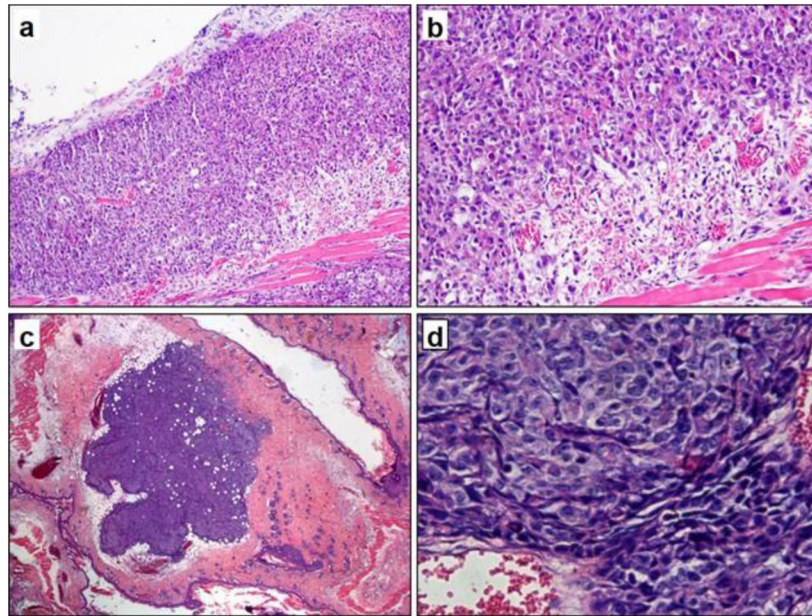


Fig. 7. H&E stained histological sections of mouse skin and tumor tissue within the window chamber corresponding to the two mice in Fig. 6. **Top row:** DSWC with implanted HCT116 cells (**a**: 100X; **b**: 200X). **Bottom row:** DSWC with HCT116/RFP cells (**c**: 200X; **d**: 400X). Cancer cells grew at high density in loose connective tissue. The tumor was surrounded by adipocytes and then a peripheral rim of collagen, stromal cells, and numerous newly formed capillaries.

Table 1

Biodistribution (%ID/g) of HCT116 (Group I-III) and PC3 cancer (Group IV)

Tissue	Group I ^{99m} Tc-TCP-1	Group II [†] ^{99m} Tc-TCP-1	Group III Inactive peptide	Group IV [‡] ^{99m} Tc-TCP-1
Blood	0.18±0.02	0.16±0.07	0.94±0.08 *	0.25±0.06
Tumor	1.01±0.15	0.26±0.04 *	0.23±0.01 *	0.17±0.01 *
Heart	0.13±0.05	0.22±0.14	0.30±0.01	0.24±0.03
Lung	0.29±0.07	0.61±0.43	0.46±0.02	0.41±0.04
Liver	0.53±0.12	0.50±0.17	0.81±0.04	0.74±0.17
Spleen	0.25±0.07	0.43±0.35	0.31±0.03	0.34±0.05
Stomach	0.41±0.14	0.42±0.21	0.79±0.23	0.53±0.17
Small Intestine	0.65±0.13	0.71±0.12	0.51±0.10	0.64±0.31
Large Intestine	0.46±0.10	0.26±0.04	0.92±0.20	0.53±0.19
Kidneys	7.23±2.50	3.89±0.91	17.32±1.28 *	4.78±0.71
Muscle	0.06±0.01	0.10±0.07	0.09±0.01	0.08±0.01
Skin	0.29±0.06	0.15±0.03	0.26±0.01	0.33±0.05
Tumor/Blood	5.92±0.96	2.23±0.45 *	0.25±0.02 *	0.82±0.15 *
Tumor/Muscle	16.87±0.60	6.57±1.56 *	2.56±0.08 *	2.30±0.23 *

Data were collected at 3-h post-injection.

* $P < 0.05$ compared to Group I;[†] with blockade;[‡] PC3 prostate cancer